Supporting Information for

A novel flake-like Cu_7S_4 solar absorber for high-performance large-scale water evaporation

Xuejian Li[a], Zhongping Yao[a,1], Jiankang Wang[b], Dongqi Li[a], Kailun Yu[a], Zhaohua Jiang[a]

[a] School of Chemistry and Chemical Engineering, State Key Laboratory of Urban Water Resource and Environment, Harbin Institute of Technology, Harbin, 150001, China

[b]Chongqing Key Laboratory of Extraordinary Bond Engineering and Advanced Materials Technology (EBEAM), Yangtze Normal University, Chongqing 408100, China

[1] corresponding author, email address: yaozhongping@hit.edu.cn

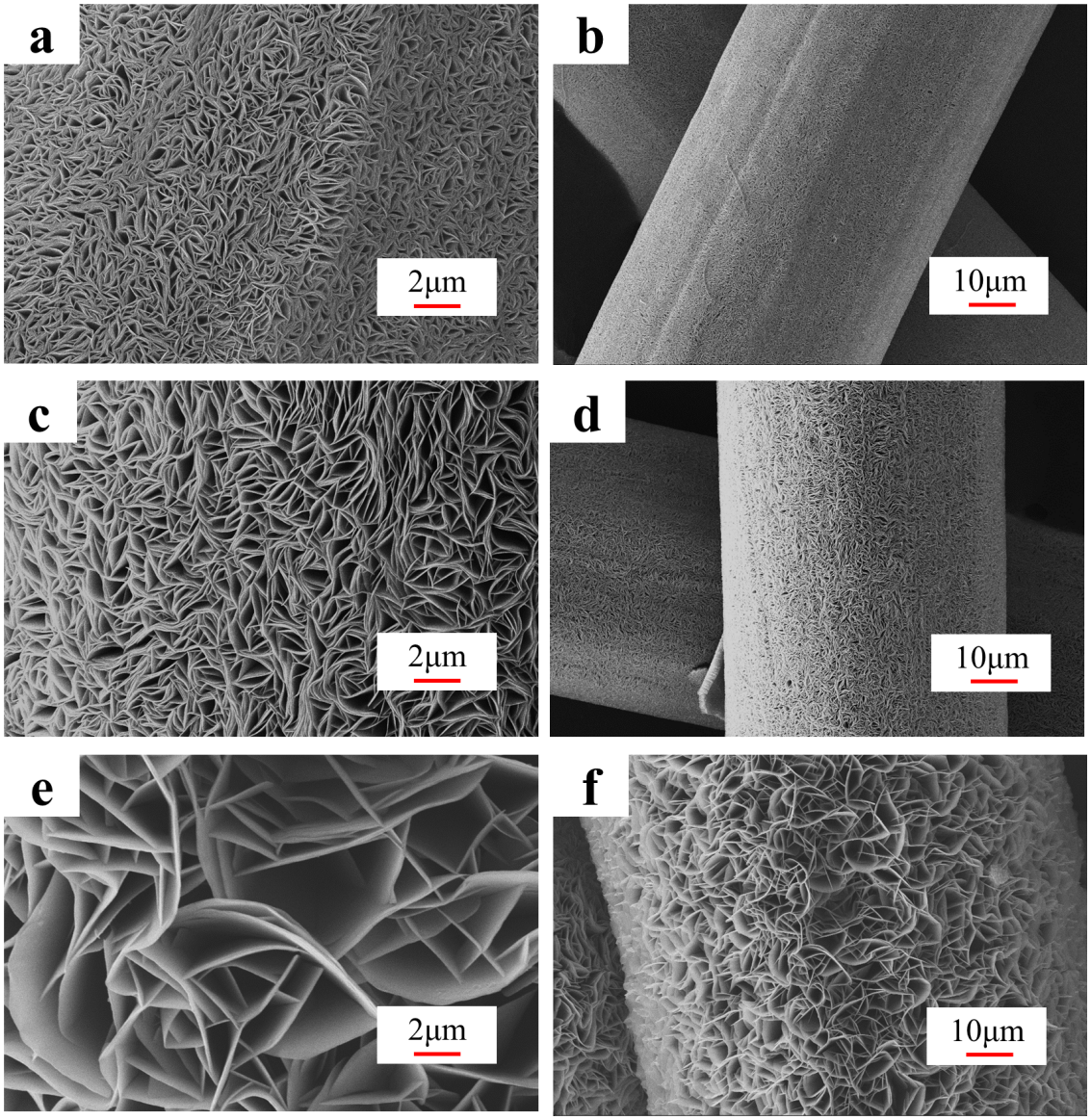

Fig.S1 SEM images of samples with different immersion time. (a, b) 10 s; (c, d) 1 min; (e, f) 10 min

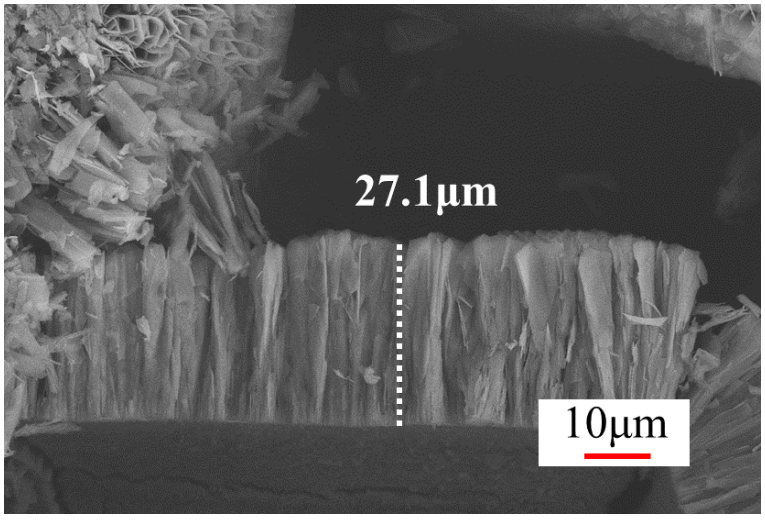

Fig.S2 Cross section of the sample prepared under immersion time of 10 minutes

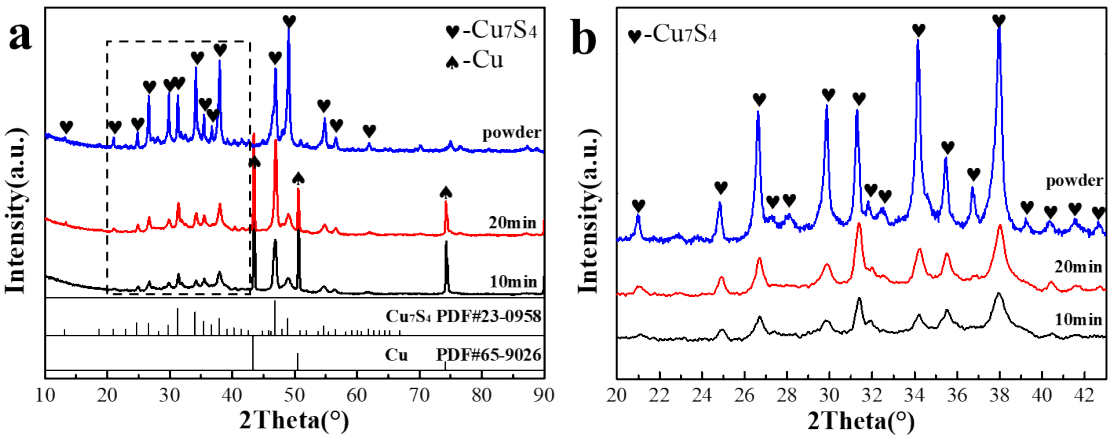

Fig.S3 (a) XRD patterns of samples with different immersion time (black powder was obtained with long enough immersion time); (b) XRD patterns with scanning angle from 20° to 43°.

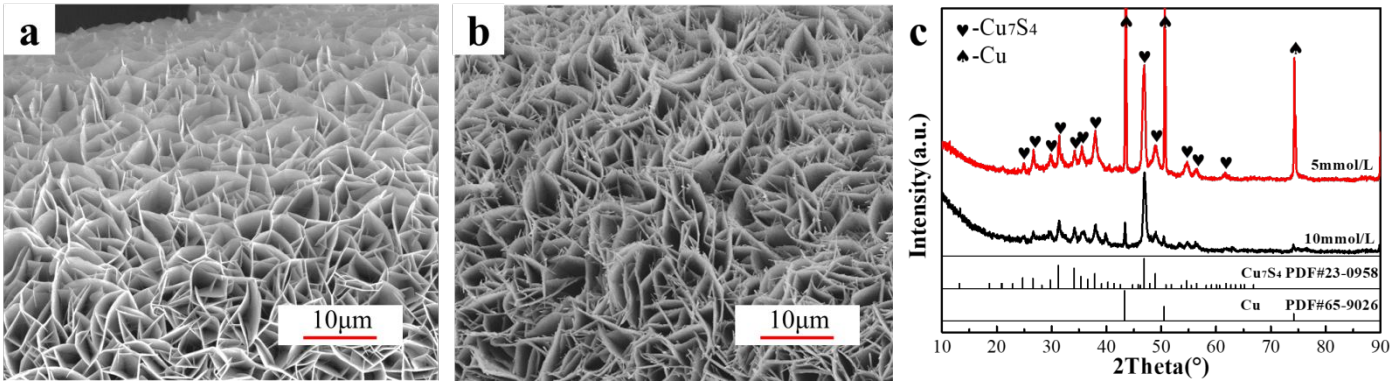

Fig.S4 (a, b) SEM images of samples with various concentration of S in the solution. (a) 5 mmol/L; (b) 10 mmol/L; (c) XRD patterns of samples with various concentration of S in the solution.

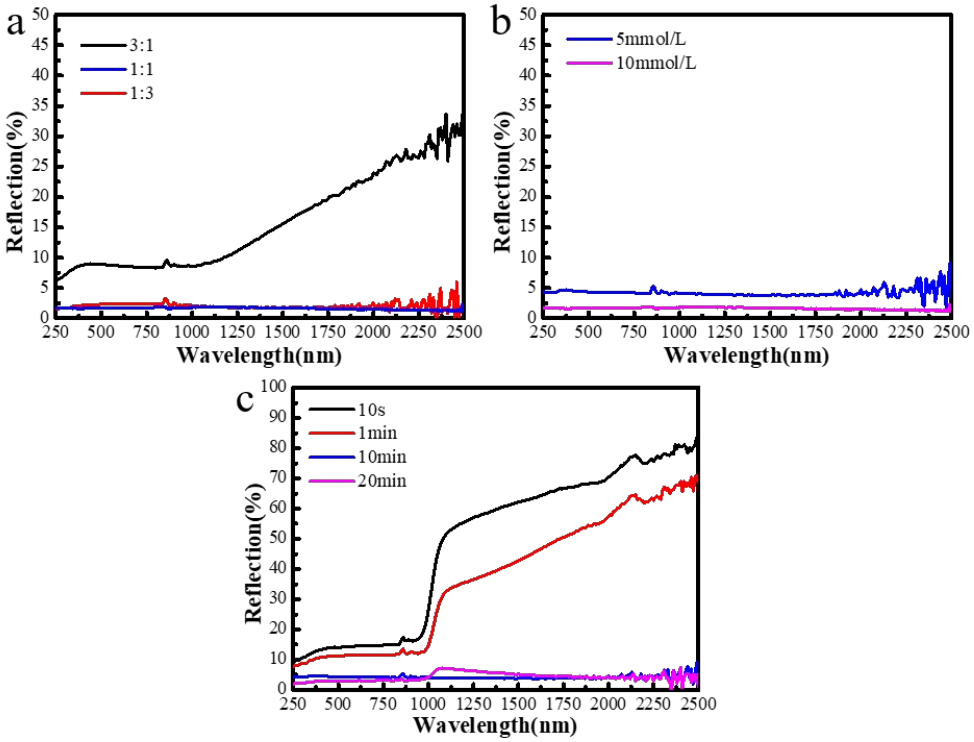

Fig.S5 Reflection spectra of samples prepared with different conditions.
(a) different S/S^{2-} ratios; (b) different concentration of S in the solution; (c) different immersion time

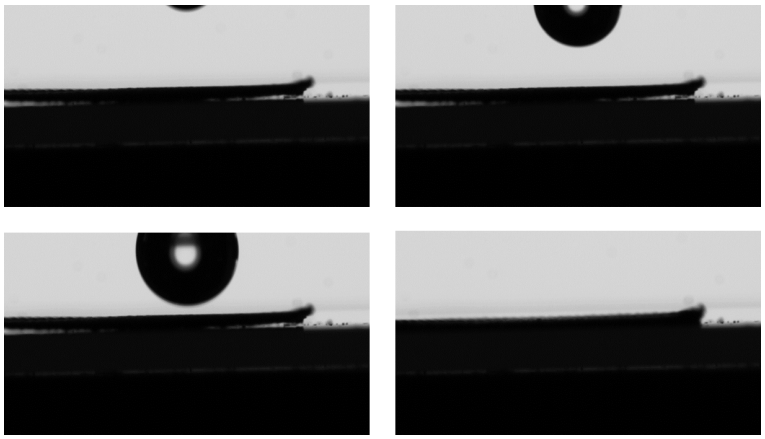

Fig.S6 Process of measurement of contact angle

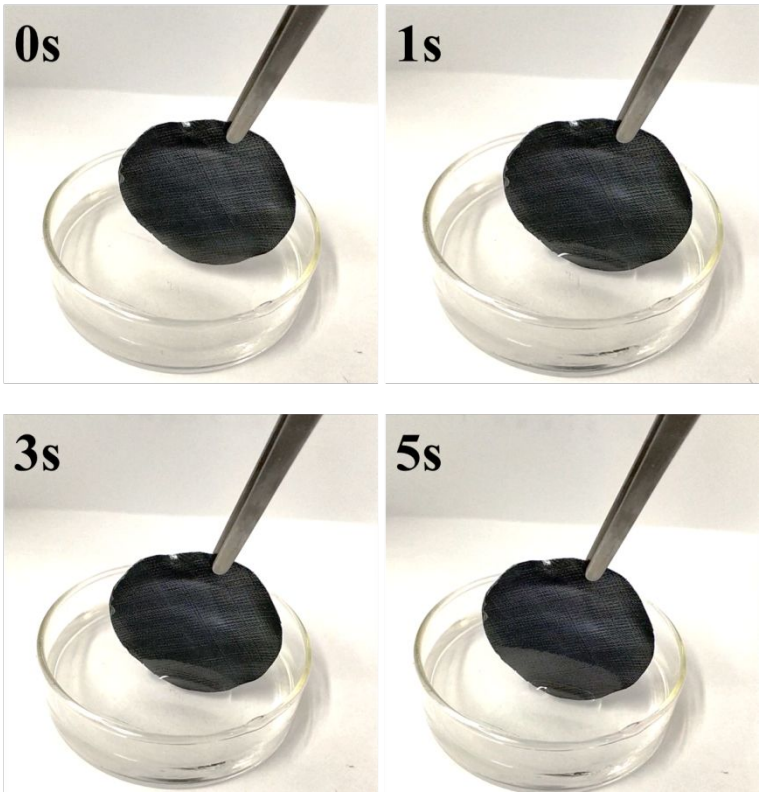

Fig.S7 Hydrophilicity verification of the sample.

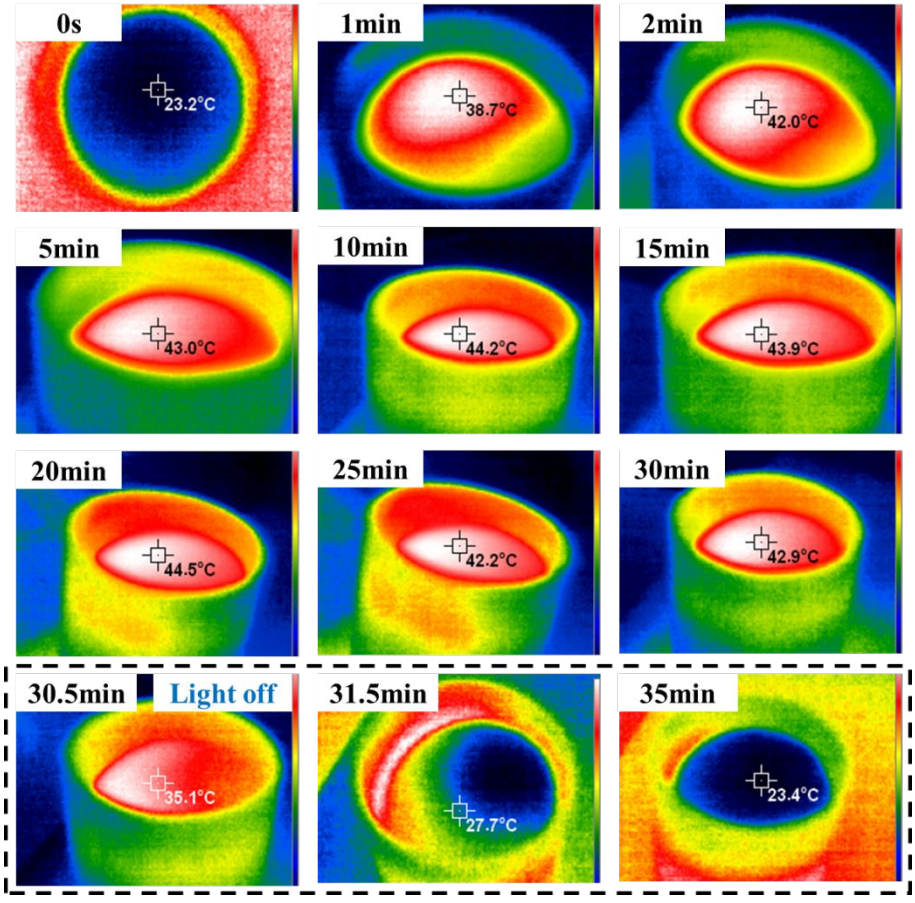

Fig.S8 Infrared photos taken by infrared imaging device during measurement of water evaporation rate.

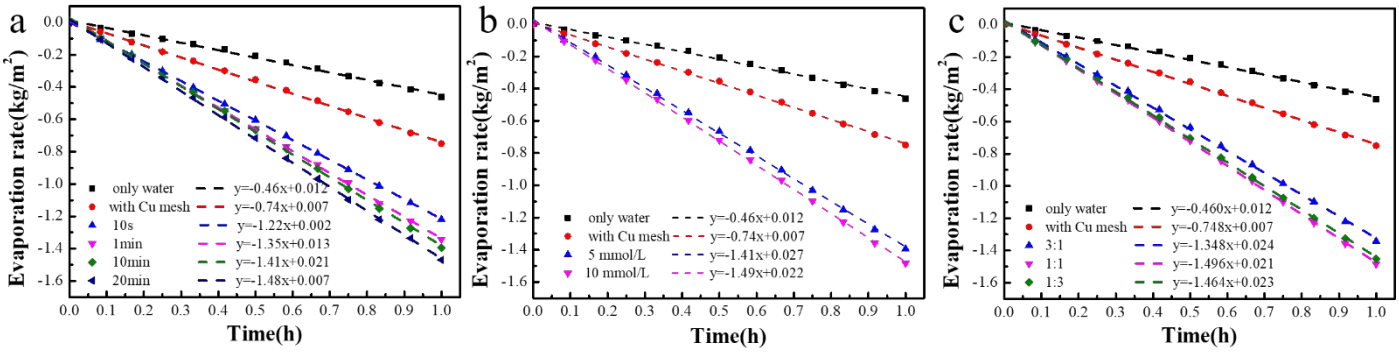

Fig.S9 Evaporation water weight versus time under 1kW/m^2 under different process conditions (a) various immersion time; (b) various concentration of S in the solution; (c) various S/S^{2-} ratios

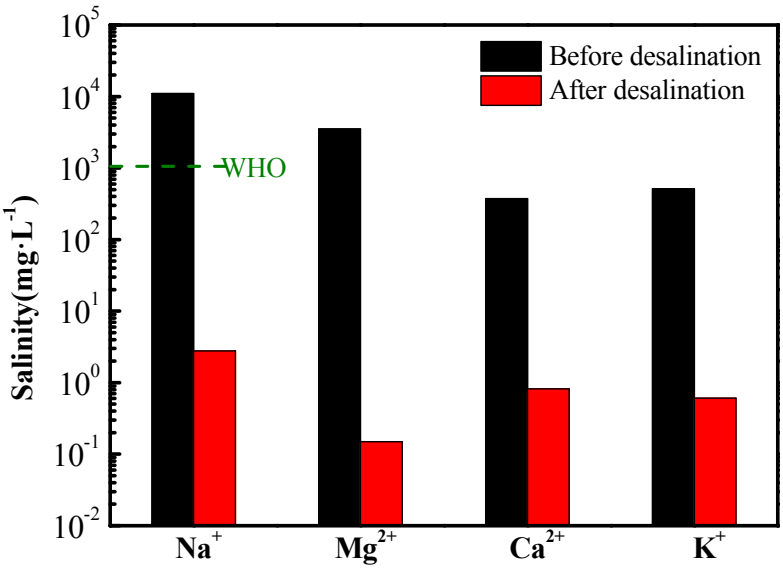

Fig.S10 The concentrations of four primary ions before and after desalination.

Table.S1 Absorptivity of sample with ranges of different wavelength

Sample	UV	Visible	NIR	Total
Solar-ideal	7%	50%	43%	100%
Cu_7S_4/Cu mesh	6.7%	47.8%	41.2%	95.7%

Table.S2 Absorptivity of different wavelength ranges under various the S/S^{2-} ratios

Sample	UV	Visible	NIR	Total
Solar-ideal	7%	50%	43%	100%
3:1	6.6%	45.6%	36.3%	88.5%
1:1	6.9%	49.2%	42.3%	98.4%
1:3	6.9%	48.8%	42.1%	97.8%

Table.S3 Absorptivity of different wavelength ranges under various concentration of S

Sample	UV	Visible	NIR	Total
Solar-ideal	7%	50%	43%	100%
5 mmol/L	6.7%	47.8%	41.2%	95.7%
10 mmol/L	6.9%	49.2%	42.2%	98.3%

Table.S4 Absorptivity of different wavelength ranges under various immersion time

Sample	UV	Visible	NIR	Total
Solar-ideal	7%	50%	43%	100%
10s	6.2%	42.9%	20.3%	69.3%
1min	6.4%	44.3%	26.3%	77.0%
10min	6.7%	47.8%	41.2%	95.7%
20min	6.8%	48.5%	41.0%	96.3%

Table S5 The comparison of photothermal evaporation performance of Cu_7S_4/Cu mesh with the reported photothermal materials

Photothermal materials	Solar absorptivity	Evaporation rate/kg·m^{-2}·h^{-1}	Conversion efficiency	Illumination intensity/ kW·m^{-2}	References
Cu7S4/Cu mesh	95.7%	1.41	88.1%	1	This work
Graphene oxide/2D water path	~94%	-	80%	1	[1]
rGO-MWCNT/ PVDF membrane	95.3%	1.22	80.45%	1	[2]
Mesoporous Wood-Based graphite	>95%	1.20	80%	1	[3]
Exfoliated graphite/carbon foam	97%	-	64%	1	[4]
Ti_2O_3 NP/cellulose membrane	92.5%	1.32	-	1	[5]
Black TiO_x/ stainless steel mesh	91.3%	0.8012	50%	1	[6]
CuS/polyethylene membrane	93%	1.02	63.9%	1	[7]
Cu_7S_4 nanocrystal film	-	-	77.1%	1.006	[8]

CuS/mixed cellulose membrane	>85%	1.12	80±2.5%	1	[9]
PPy/stainless steel mesh	-	0.92	58%	1	[10]
Au/AAO nanoporous template	99%	-	>90%	4	[11]
Au film/Airlaid paper	87%	5.5	77%	4.5	[12]
Al-Ti-O nanostructure membrane	90.32%	1.03	77.52%	1	[13]
Black gold membrane	91%	-	57	20	[14]
Al/AAO membrane	96%	0.92	58%	1	[15]

Discussion of calculation on the energy loss in the evaporation system

Radiation and convection towards the ambient environment are the two main factors of energy loss during the process of solar steam generation. The radiation and convection loss can be calculated by equations below:

Radiation: $\Phi = \varepsilon\sigma(T_1^4 - T_2^4)$

Convection: $Q = h(T_1 - T_2)$

where ε is the emissivity of the material (assumed to be 1), σ Stefan-Boltzmann constant (5.67×10^{-8} $W\cdot m^{-2}\cdot K^{-4}$), h the convection heat transfer coefficient (about 10 $W\cdot m^{-2}\cdot K^{-1}$), T_1 the temperature of interface (43.5 ℃ in this work), and T_2 the temperature of ambient environment.

There is a film of water and surrounded vapor around the interface during the process of solar evaporation and the temperature of the vapor film is close to the surface temperature, which has been proved by many reports[4, 16-17] (e.g. 2.6 ℃ in Reference 11). The thermal energy generated by the absorbing materials would exchange energy in this small area at first, instead of directly emitting thermal radiation and exchange heat with the surroundings through the convection[17]. Therefore, the radiation and convection loss are small. In this way, the temperature of the ambient environment (T_2) is about 40.9 ℃. After calculation by the equations above, the loss in the evaporation system is only 1.9% by radiation and 2.6% by convection.

References

1. Li, X.; Xu, W.; Tang, M.; Zhou, L.; Zhu, B.; Zhu, S.; Zhu, J., Graphene oxide-based efficient and scalable solar desalination under one sun with a confined 2D water path. *Proceedings of the National Academy of Sciences* **2016,** *113* (49), 13953-13959.

2. Wang, Y.; Wang, C.; Song, X.; Megarajana, S. K.; Jiang, H., A facile nanocomposite strategy to fabricate a rGO–MWCNT photothermal layer for efficient water evaporation. *Journal of Materials Chemistry A* **2017,** *74* (8), 972-978.

3. Li, T.; Liu, H.; Zhao, X.; Chen, G.; Dai, J.; Pastel, G.; Jia, C.; Chen, C.; Hitz, E.; Siddhartha, D., Scalable and Highly Efficient Mesoporous Wood‐Based Solar Steam Generation Device: Localized Heat, Rapid Water Transport. *Advanced Functional Materials* **2018**, 1707134-1707142.

4. Ghasemi, H.; Ni, G.; Marconnet, A. M.; Loomis, J.; Yerci, S.; Miljkovic, N.; Chen, G., Solar steam generation by heat localization. *Nature Communications* **2014,** *5* (5), 4449-4456.

5. Wang, J.; Li, Y.; Deng, L.; Wei, N.; Weng, Y.; Dong, S.; Qi, D.; Qiu, J.; Chen, X.; Wu, T., High‐Performance Photothermal Conversion of Narrow‐Bandgap Ti2O3 Nanoparticles. *Advanced Materials* **2016,** *29* (3), 1603730.

6. Ye, M.; Jia, J.; Wu, Z.; Qian, C.; Chen, R.; O'Brien, P. G.; Sun, W.; Dong, Y.; Ozin, G. A., Synthesis of black TiOx nanoparticles by Mg reduction of TiO2 nanocrystals and their application for solar water evaporation. *Advanced Energy Materials* **2017,** *7* (4), 1601811.

7. Shang, M.; Li, N.; Zhang, S.; Zhao, T.; Zhang, C.; Liu, C.; Li, H.; Wang, Z., Full-

Spectrum Solar-to-Heat Conversion Membrane with Interfacial Plasmonic Heating Ability for High-Efficiency Desalination of Seawater. *Applied Energy Materials* **2018,** *1* (1), 56-61.

8. Zhang, C.; Yan, C.; Xue, Z.; Yu, W.; Xie, Y.; Wang, T., Shape‐Controlled Synthesis of High‐Quality Cu7S4 Nanocrystals for Efficient Light‐Induced Water Evaporation. *Small* **2016,** *12* (38), 5320-5328.

9. Guo, Z. G.; Xin, M.; Gang, W.; Hou, B.; Wang, X., Super-hydrophilic copper sulfide films as light absorbers for efficient solar steam generation under one sun illumination. *Semiconductor Science Technology* **2017,** *33* (2).

10. Zhang, L.; Tang, B.; Wu, J.; Li, R.; Wang, P., Hydrophobic Light-to-Heat Conversion Membranes with Self-Healing Ability for Interfacial Solar Heating. *Advanced Materials* **2015,** *27* (33), 4889-4894.

11. Zhou, L.; Tan, Y.; Ji, D.; Zhu, B.; Zhang, P.; Xu, J.; Gan, Q.; Yu, Z.; Zhu, J., Self-assembly of highly efficient, broadband plasmonic absorbers for solar steam generation. *Science Advances* **2016,** *2* (4), e1501227-e1501227.

12. Liu, Y.; Yu, S.; Feng, R.; Bernard, A.; Liu, Y.; Zhang, Y.; Duan, H.; Shang, W.; Tao, P.; Song, C., A Bioinspired, Reusable, Paper-Based System for High-Performance Large-Scale Evaporation. *Advanced Materials* **2015,** *27* (17), 2768-2774.

13. Yi, L.; Ci, S.; Luo, S.; Shao, P.; Hou, Y.; Wen, Z., Scalable and Low-cost Synthesis of Black Amorphous Al-Ti-O Nanostructure for High-efficient Photothermal Desalination. *Nano Energy* **2017,** *41*, 600-608.

14. Bae, K.; Kang, G.; Cho, S. K.; Park, W.; Kim, K.; Padilla, W. J. A.-O. h. o. o., Flexible thin-film black gold membranes with ultrabroadband plasmonic nanofocusing for efficient solar vapour generation. (2041-1723 (Electronic)).

15. Zhou, L.; Tan, Y.; Wang, J.; Xu, W.; Yuan, Y.; Cai, W.; Zhu, S.; Zhu, J., 3D self-assembly of aluminium nanoparticles for plasmon-enhanced solar desalination. *Nature Photonics* **2016,** *10* (6), 393-340.

16. Ni, G.; Li, G.; Boriskina, S. V.; Li, H.; Yang, W.; Zhang, T. J.; Chen, G., Steam generation under one sun enabled by a floating structure with thermal concentration. *Nature Energy* **2016,** *1*, 16126-16133.

17. Liu, Z.; Song, H.; Ji, D.; Li, C.; Cheney, A.; Liu, Y.; Zhang, N.; Zeng, X.; Chen, B.; Gao, J., Extremely cost ‐ effective and efficient solar vapor generation under nonconcentrated illumination using thermally isolated black paper. *Global Challenges* **2017,** *1* (2), 1600003.